Nanoscale

PAPER

View Article Online
View Journal | View Issue



Cite this: *Nanoscale*, 2019, **11**, 955

# Dichotomy between frustrated local spins and conjugated electrons in a two-dimensional metal–organic framework†

Wei Jiang, [a,b] Zheng Liu,*[c] Jia-Wei Mei,*[d] Bin Cui [e] and Feng Liu*[a]

Received 19th October 2018,
Accepted 20th November 2018

DOI: 10.1039/c8nr08479c

rsc.li/nanoscale

Dichotomy between local spins and conjugated electrons spawns various exotic physical phenomena, however, it has mostly been reported in three-dimensional (3D) inorganic systems. We show, for the first time, that a rare 2D metal–organic framework exhibits intriguing dichotomy behavior, which can be directly identified through scanning tunneling microscopy/spectroscopy (STM/STS). In a newly synthesized Cu-hexaiminobenzene [$Cu_3(HAB)_2$], on the one hand, the $Cu^{2+}$ ions form an ideal $S - 1/2$ antiferromagnetic (AFM) kagome lattice; on the other hand, the conjugated-electrons from the organic ligands produce a frustrated $\pi_{x,y}$ model on a honeycomb lattice, giving rise to completely dispersionless energy bands around the Fermi level that favour the ferromagnetic (FM) state. Remarkably, the frustrated local spins and conjugated electrons interact through a strong FM Hund's coupling, giving rise to a wide range of intriguing quantum phases. Furthermore, we propose that this dichotomy can be directly characterized through STM/STS measurements due to its special 2D nature, which provides a unique exciting platform to investigate the dichotomy of frustrated spins and electrons in a single lattice.

## Introduction

The coexistence and competition of local spins and conducting electrons is one of the most fascinating problems in condensed matter physics. Such a dichotomy between electronic localization and itinerancy leads to a range of intriguing physical phenomena in strongly correlated systems, such as the Kondo system,[1,2] the heavy fermion system,[3,4] cuprate and iron pnictide high temperature superconductors,[5–8] and giant magnetoresistance (GMR) systems.[9–11] The entanglement between spin and charge degrees of freedom in these dichotomy systems spawns exotic condense matter phases that have attracted much attention for fundamental studies (*e.g.*, quantum critical phenomena and unconventional superconductivity) and also for potential applications (*e.g.*, GMR and spintronics). So far, studies of dichotomy physics have been confined to inorganic systems, which are mostly in 3D forms. Generally, dichotomy features in these systems are not directly observable, but instead are revealed indirectly through their measurable physical manifestations, *e.g.*, superconductivity and GMR effect. As a consequence, the underlying mechanisms for many observed phenomena remain mysterious, leading inevitably to controversies between experimental results and theories.

On the other hand, rapid development in modern chemical synthesis is turning metal–organic frameworks (MOFs)[12–14] into a playful Legoland,[15–17] where structures with desired electronic and magnetic properties can be delicately tailored with diverse metal ions and organic linkers.[18–20] Recently, 2D MOFs have been successfully synthesized[21–23] and many interesting phenomena have been proposed.[24–28] Here, we demonstrate that 2D MOFs represent a novel promising platform to study the dichotomy between local spins and itinerant electrons, because of the coexistence and competition between the spin degrees of freedom from metal ions and π-conjugated itinerant electrons from organic ligands. Most remarkably, we show that the dichotomy feature of 2D MOFs can be directly identified experimentally, which provides a distinct advantage over 3D inorganic systems.

As a prototypical model system, we use a recently synthesized Cu-hexaiminobenzene framework [$Cu_3(HAB)_2$,

[a]Department of Materials Science and Engineering, University of Utah, Salt Lake City, Utah 84112, USA. E-mail: fliu@eng.utah.edu
[b]Department of Electrical and Computer Engineering, University of Minnesota, Minneapolis, Minnesota 55455, USA
[c]Institute for Advanced Study, Tsinghua University, Beijing 100084, China. E-mail: zheng-liu@mail.tsinghua.edu.cn
[d]Institute for Quantum Science and Engineering, and Department of Physics, Southern University of Science and Technology, Shenzhen 518055, China. E-mail: meijw@sustc.edu.cn
[e]School of physics, Shandong University, Jinan 250100, China

†Electronic supplementary information (ESI) available. See DOI: 10.1039/C8NR08479C

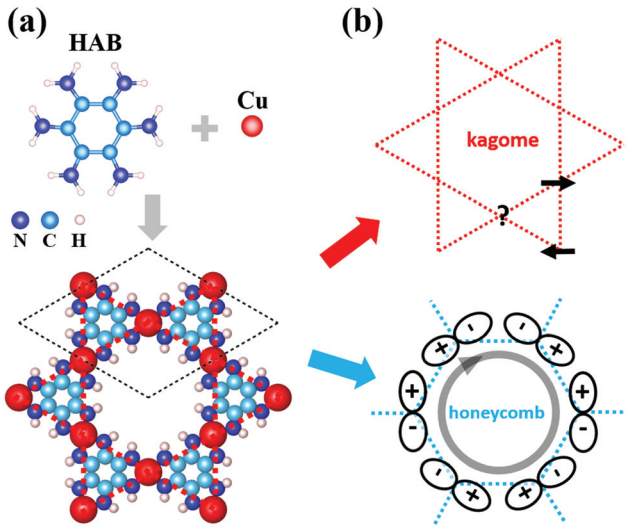


**Fig. 1** Structural and electronic properties of $Cu_3(HAB)_2$. (a) Atomic structure of a HAB molecule and the crystalline structure of $Cu_3(HAB)_2$ by coordinating HAB with Cu. (b) Schematics of two frustrations in this material.

$Cu_3(C_6N_6H_6)_2$][29,30] to elaborate on our findings. As schematically shown in Fig. 1(a), the HAB ligands connect Cu ions into a 2D periodic lattice; each Cu ion locally coordinates with four N atoms in a distorted planar square geometry. We reveal that this material can be viewed as a combination of two subsystems [Fig. 1(b)]. One is a kagome antiferromagentic $S = 1/2$ lattice (KAFM) consisting of $Cu^{2+}$ ions. The other subsystem consists of $p_{x,y}$-like ($\pi_{x,y}$) molecular orbitals on a honeycomb lattice that gives rise to an itinerant flat band right at the Fermi level. Remarkably, the two subsystems are simultaneously frustrated and also strongly coupled within a close energy proximity, representing the first organic dichotomy system with possibly new condensed-matter phases with different amounts of doping. We note that though localized spins and the singlet biradical have been reported in bis(benzene-1,2-dithiolato)metal molecular complexes,[31–34] it is different from a dichotomy system as the competition between the two characteristic electrons does not exist without crystal periodicity. Though it broadly exists in MOFs,[23,29,30] to the best of our knowledge, no literature studies have reported such a phenomenon yet.

We implement two methods, (i) doping and (ii) tuning correlation strength ($U$), to study the competition between localized spins (AFM) and itinerant electrons (FM), based on which a phase diagram is constructed for different doping levels and correlation strengths. Most importantly, beyond traditional 3D inorganic dichotomy systems, we further demonstrate that the dichotomy substantiated in 2D $Cu_3(HAB)_2$ can be directly identified through scanning tunneling microscopy/spectroscopy (STM/STS) measurements. Furthermore, as one of the well-known outcomes due to the dichotomy, the GMR effect in $Cu_3(HAB)_2$ is analyzed with the formation of a magnetic polaron due to frustration.

## Calculation results

We first calculated the band structure within the standard density functional theory (DFT, see computational details in ESI†) [Fig. 2(a)]. Below the Fermi level (from −1.75 to −0.5 eV), there is a pair of isolated $\pi_z$ Dirac bands just like the $p_z$-bands in graphene. Around the Fermi level (−0.25 to 0.5 eV), there are seven bands, among which three are completely dispersionless, manifesting typical features of frustration. More importantly, the Fermi level almost coincides with one of the flat bands.[25,26,35] By resolving these bands according to the atomic composition, they can be decomposed into a three-band set (red) and a four-band set (blue). The three-band set mainly arises from the Cu ions, which can be nicely fitted by a single-orbital tight-binding (TB) hopping model on a kagome lattice [Fig. 2(b)]:

$$H_{\mathrm{d}}^{\circ} = t_{\mathrm{d}} \sum_{\langle ij \rangle} (\mathrm{d}_{i\sigma}^{\dagger} \mathrm{d}_{j\sigma} + \mathrm{H.c.}) \quad (1)$$

where the summation $\langle ij \rangle$ are constrained within the nearest-neighbors (NN) on the Cu kagome lattice indexed by $i$, $j$, and $t_{\mathrm{d}} = 0.06$ eV is the fitted NN hopping amplitude. The four-band set arises from a combination of N and C orbitals, reflecting the typical features of an effective $\pi_{xy}$ σ-bond hopping model on a honeycomb lattice:

$$H_{\pi}^{\circ} = t_{\pi} \sum_{\langle IJ \rangle} (\pi_I^{\dagger} \pi_J^{l} + \mathrm{H.c.}) \quad (2)$$

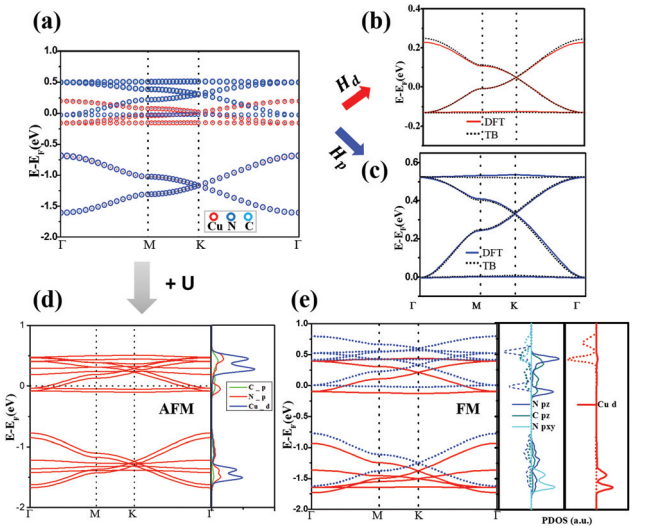


**Fig. 2** Band structures from DFT, DFT+U and the effective TB models. (a) Atomic-resolved DFT band structure; the marker size indicates the weight of the atomic composition. Decomposition of the bands into (b) a kagome lattice and (c) a honeycomb lattice, with comparison to the effective TB model band structure. (d) The DFT+U AFM band structure and the projected density of states (PDOS). (e) The DFT+U FM band structure and PDOS. The solid and dashed curves correspond to different spins.

where the summation $\langle IJ\rangle$ are constrained within the NN bonds on the HAB honeycomb lattice indexed by $I$, $J$. $\pi^{l\dagger}$ creates a superposition state of $\pi_x$ and $\pi_y$ orbitals with the orbital vector parallel to the bond, *i.e.*, $|\pi^l\rangle = \cos\phi|\pi_x\rangle + \sin\phi|\pi_x\rangle$ with $\phi$ as the angle between the bond and the $x$-axis. $\pi_{x,y}$ are molecular conjugated orbitals from HAB with analogical symmetries to atomic $p_{x,y}$ orbitals. According to Fig. 2(a), they distribute among both C and N atoms. In this model, $t_\pi$ is equivalent to the σ-bond hopping amplitude, while the weak π-bond hopping is neglected. $t_\pi$ is fitted to be 0.22 eV [Fig. 2(c)]. We noticed that the LDA band structure could be better reproduced by further considering the small $\pi^l$-orbitals overlap on the NN sites $S = \langle\pi_I^l|\pi_J^l\rangle = 0.18$. The generalized eigenvalue problem becomes $\det\ (H_\pi^\circ - \varepsilon S) = 0$, where $\varepsilon$ is the eigenenergy.

To fully characterize this intriguing material beyond DFT, two additional questions should be answered: (a) What is the basis of these hopping models? The nonorthogonality of the effective $\pi_{x,y}$-orbitals revealed from the band fitting already implies that they should be complicated molecular orbitals; (b) How does correlation interaction change the picture? This question is particularly important to the kagome bands arising from Cu, because Cu 3d-electrons are known to experience strong Coulomb repulsion.

These questions can be partially addressed by studying the building blocks of $Cu_3(HAB)_2$ based on the quantum chemistry computational package (Gaussian). We proceed by a "computational thought experiment" to analyze first a single HAB molecule [Fig. 3(a)], then a Cu-$(HAB)_2$ complex formed by sandwiching one Cu atom between two HAB molecules [Fig. 3(b)], and finally a crystalline $Cu_3(HAB)_2$ by imposing the periodic boundary condition (PBC) [Fig. 3(c)]. Fig. 3(d) shows the three highest occupied molecular orbitals (HOMOs) of a single HAB molecule with the corresponding wavefunction of these orbitals. It is clear that they mainly arise from the π-conjugation of the C/N $p_z$-orbitals. The two degenerate levels ($\pi_x$ and $\pi_y$) on top have the same symmetry as the atomic $p_x$ and $p_y$ orbitals. The single level below ($\pi_z$) has the same symmetry as the atomic $p_z$ orbital. The molecular $\pi_{x,y}$-orbitals define the basis of eqn (2). In a single molecule, $\pi_{x,y,z}$ are all fully occupied.

Fig. 3(e) (left panel) shows the evolution of the occupied levels after putting a Cu atom between two HAB molecules. The HOMO now becomes a half-filled single orbital primarily consisting of the Cu 3d orbital (SOMO). By choosing the coordinates in Fig. 3(b) as the orbital quantization axes, this MO is equivalent to an atomic $d_{xy}$-orbital. All the other Cu 3d-orbitals are found to be deep down away from the Fermi level and fully occupied. Hence, Cu is in a +2 ($3d^9$) valence state, containing one single hole. The situation is actually very similar to that in high-$T_c$ cuprate superconductors,[6] where the Cu–O planar crystal field splits out a half-filled $d_{xy}$-orbital, and the dynamics of this dangling bond is the microscopic origin of all the unusual electronic properties.[6]

The $\pi_{x,y}$ orbitals now become the second HOMOs (HOMO–$n$). They are still degenerate, but the filling factor reduces from 1 to $\frac{3}{4}$ [left panel of Fig. 3(e)]. This result can be understood by noticing that to bond with Cu, the two HAB molecules release four $H^+$ ions in total. The $Cu^{2+}$ ion, however, can only donate two electrons to the HAB molecules. Consequently, upon bonding with a Cu, each HAB molecule loses one out of its four $\tilde{p}_{x,y}$ electrons. It is worth noting that the two floating π electrons in Cu-$(HAB)_2$ have been extensively studied,[31,32,34] where the singlet biradical state with two singly occupied states was proved to be more stable than the resonance state with one single HOMO level occupied by two elec-

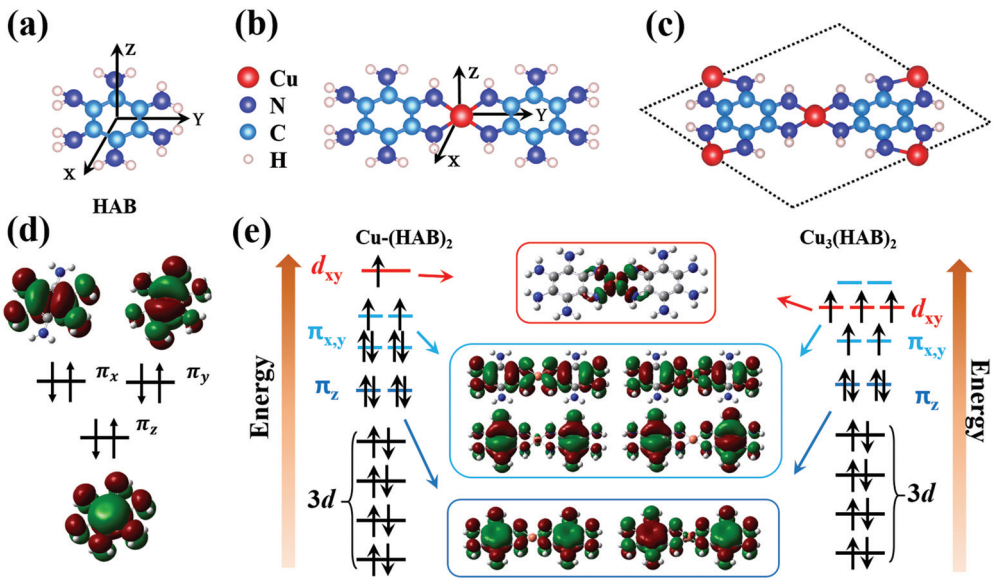


**Fig. 3** Molecular information. (a) HAB molecule. (b) Cu-$(HAB)_2$ complex. (c) $Cu_3(HAB)_2$ crystal. (d) Wavefunctions of HAB molecule. (e) Energy levels and the associated wavefunctions of (b) a Cu-$(HAB)_2$ complex (left) and (c) $Cu_3(HAB)_2$ crystal (right).

trons. Moreover, the localized spin of the $Cu^{2+}$ ion and the ligand radicals coexist and are coupled ferromagnetically because of the strict orthogonality between the two.[32] After imposing PBC with two extra Cu ions per unit cell, two HAB molecules become one-fourth filled and three Cu ions contribute three half-filled $d_{xy}$-orbitals [right panel of Fig. 3(e)] (see the discussion in the ESI and Fig. S1†). These molecular orbitals are actually the wavefunction bases forming the corresponding crystal band structures. We further performed band-resolved partial charge density calculation and maximally localized Wannier functions fitting (see the discussion in the ESI and Fig. S2†), which agree perfectly with our molecular calculation results.

We can now re-evaluate the DFT results. The effective four-band model on a honeycomb lattice (eqn (2)) can be firmly constructed out of the $\pi_{x,y}$ orbitals. These orbitals are itinerant, and thus should be well captured by DFT. The filling factor of the four-band set is $\frac{1}{4}$ (see the discussion in the ESI and Fig. S1†), which means that the bottom flat band is fully occupied and all the other three bands are empty. The location of the Fermi level calculated from LDA correctly captures this property. The origin of the flat band lies in a special localized eigenstate as sketched in Fig. 1(b). Electrons in this eigenstate cannot leak outside the hexagon due to complete destructive interference.[36]

With respect to the kagome degrees of freedom, the Cu-$(HAB)_2$ cluster calculation indicates that each $Cu^{2+}$ ion contains a local spin, whereas the DFT calculation suggests the formation of a nonmagnetic metal with the Fermi level crossing the half-filling energy. This is the widely known failure of DFT due to the underestimation of electron correlation. A simple remedy within the DFT formalism is to include electron correlations in a Hartree–Fock mean-field manner, known as the +U correction. It has been demonstrated that DFT+U can correctly reproduce the Mott insulating gap by explicitly breaking the time-reversal symmetry.[37] After testing different $U$ values,[37,38] we choose a representative $U \sim 5$ eV to demonstrate the correlated d electrons. Fig. 2(d) shows the resulting band structure with AFM coupled $Cu^{2+}$ ions. By referring to the projected density of states (PDOS) [Fig. 2(d)], we found that the Cu kagome band is split into a set of lower Hubbard bands and a set of upper Hubbard bands. The Mott gap ($U_0$) is about 2 eV, much smaller than $U \sim 5$ eV. It reflects the strength of onsite Coulomb repulsion in the presence of Coulomb screening due to itinerant conjugated π-electrons in the system. The complete Hamiltonian for this $Cu^{2+}$ degree of freedom can then be revised into:

$$H_{\mathrm{d}} = H_{\mathrm{d}}^{\circ} + U_0 \sum_I n_{i\uparrow} n_{i\downarrow}. \tag{3}$$

The hopping amplitude $t_{\mathrm{d}} = 0.06$ eV in $H_{\mathrm{d}}^{\circ}$ is much smaller than $U_0$. Therefore, at half filling, the large-$U$ perturbation can be applied, which maps $H_{\mathrm{d}}$ into an $S - \frac{1}{2}$ Heisenberg model:

$$H_{\mathrm{d}} \simeq J_{\mathrm{d}} \sum_{\langle ij \rangle} \mathbf{S}_i \cdot \mathbf{S}_j, \tag{4}$$

where $J_{\mathrm{d}} = \frac{4{t_{\mathrm{d}}}^2}{U_0} \simeq 7$ meV is the strength of the AFM NN spin exchange. This AFM superexchange strength is small because of the large distance between $Cu^{2+}$ ions. Furthermore, the $\pi_{x,y,z}$ molecular orbitals around the Fermi level primarily arise from the C/N atomic $p_z$ orbitals, which are orthogonal to the $d_{xy}$-orbital. Thus, there is no charge transfer between $\pi_{x,y}$ orbitals on HAB ligands and $d_{xy}$-orbital on Cu ions (see the discussion in the ESI and Fig. S3†). For the same reason, the superexchange for Cu 3d orbitals is scaled by on-site Coulomb interaction $U_0$.

To study the interaction between localized spins and itinerant electrons, we plotted the band structure with the metastable FM state in Fig. 2(e). One important point revealed is that a Zeeman splitting of the $\pi_{xyz}$ bands occurs. This splitting is not related to the instability of the $\pi_{xy}$ flat band, because the $\pi_z$ Dirac bands are also split of the same amount. Therefore, it should be attributed to the coupling with the Cu local spin. It is clear from Fig. 2(e) that the downshifted (upshifted) $\pi_{xyz}$ bands have the same (opposite) spin direction as the Cu spin, indicating an FM coupling. This is due to the strict orthogonality between the π spins and $d_{xy}$ spins,[32] which rules out the "double-exchange-like" interaction. Considering the hybridization between π electrons and $d_{xz,yz}$ orbitals, this can be viewed as a d–d Hund's coupling:

$$H_{\pi\mathrm{d}} = -J_{\mathrm{H}} \sum_i \sum_{I \in \mathrm{NN}(i)} \mathbf{S}_i \cdot \mathbf{s}_I, \tag{5}$$

where $\mathbf{S}_i$ and $\mathbf{s}_I = \sum_{\alpha=x,y}^{\sigma=\uparrow/\downarrow} \sigma \pi_{I\alpha\sigma}^{\dagger} \pi_{I\alpha\sigma}$ are the spin operators of the Cu $d_{xy}$ and the NN HAB $\pi_{xy}$ electrons, respectively. $J_{\mathrm{H}}$ denotes the Hund's coupling strength, which is roughly of the same magnitude as the Zeeman splitting ~100 meV.

## Dichotomy between local spins and conjugated electrons

Combining the results above, we arrive at a full effective Hamiltonian characterizing this unique material:

$$H = H_{\pi}^{\circ} + H_{\mathrm{d}} + H_{\pi\mathrm{d}}, \tag{6}$$

in which the kagome local spins described by $H_{\mathrm{d}}$ favor AFM coupling, while conjugated electrons described by $H_{\pi}^{\circ}$ favor the FM state. Interacting through the FM Hund's coupling $H_{\pi\mathrm{d}}$, the competition between d and π electrons gives rise to various intriguing quantum states. This competition is systematically studied by hole doping and parameter $U$ variations using the DFT+U approach. The former is experimentally feasible through either the gating or chemical redox control method,[39–41] and the latter can be realized by metal ion substitution. Based on our DFT calculations, a phase diagram in the parameter space of hole concentration and $U$ (LDA + $U$) is created, as shown in Fig. 4(a). The system changes from AFM to FM state with the increase of $U$ [see blue dashed arrow in

 

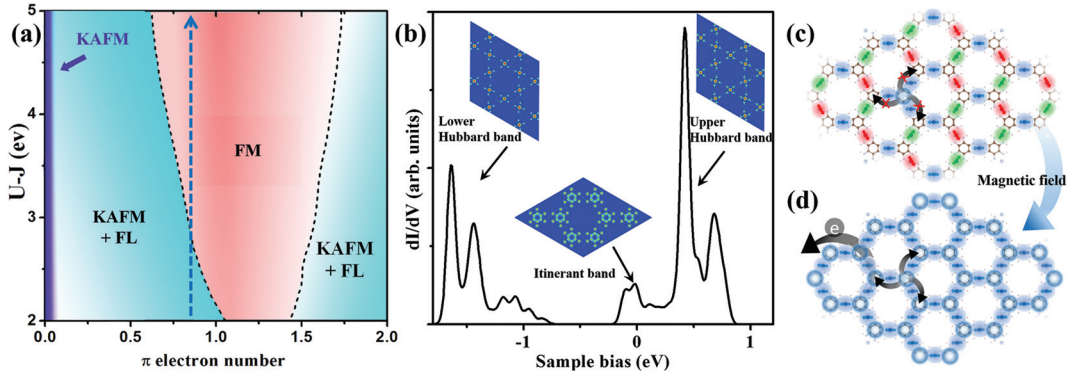


Fig. 4 Dichotomy between local spins and itinerant electrons. (a) Phase diagram in the parameter space of hole concentration and $U$ (LDA + $U$). (b) d$I$/d$V$ spectra simulated for $Cu_3(HAB)_2$ surface with two prominent Hubbard peaks below and above the Fermi level along with one itinerant peak at the Fermi level. The insets show the STM topography of $Cu_3(HAB)_2$ surface with bias of 0.45/−1.55 and 0 eV corresponding to the kagome upper/lower Hubbard and honeycomb itinerant band, respectively. (c) Formation of magnetic polaron under kagome AFM background. (d) FM spin configuration under magnetic field.

Fig. 4(a)], consistent with the inversely proportional relationship between AFM strength $J_d = \frac{4t_d^2}{U_0}$ and $U_0$ (see the discussion in the ESI and Table S1†). We also calculated the system using GGA + $U$ in comparison with that from LDA + $U$. The results show that with the same $U$ value, GGA + $U$ tends to amplify the FM state compared to LDA + $U$ (see Table S2 in the ESI†).

The phase evolution with hole doping is more intriguing. With different amounts of π electrons, the system could possibly hold KAFM, KAFM plus Fermi liquid, and FM states [Fig. 4(a), see also the discussion in the ESI and Fig. S4†]. We note that the FM phase may be overestimated for both LDA + $U$ and GGA + $U$, because of the drawback of mean-field based DFT calculations. A more accurate phase diagram of the dichotomy system can be obtained through many-body calculations, such as DMFT or VMC. It is also interesting to mention that the full Hamiltonian resembles that of the "frustrated Kondo system", which is a long-standing subject in the frustrated magnetism community.[42–44] However, these studies are beyond the scope of this work. The main goal of this paper is to demonstrate and propose feasible experimental approaches to characterize the dichotomy phenomenon in MOFs, which we believe can be well captured by DFT calculations.

To directly identify the two frustrated degrees of freedom, we propose to perform STM/STS measurements of $Cu_3(HAB)_2$ experimentally, which has been proved accessible growing and studying 2D monolayer metal–organic coordinated systems.[45–47] More recently, 2D honeycomb MOFs have been successfully grown on a weakly interacting graphene substrate,[48] which makes exploring intrinsic properties of monolayer $Cu_3(HAB)_2$ through STM feasible and promising. We note that this proposal is solely for 2D MOFs grown on substrates than 3D MOFs or 2D MOFs in the 3D form. Additionally, the dramatically different structural motifs of metal ion *versus* ring of organic ligands provide a pronounced contrast to efficiently distinguish the two kinds of electrons, *i.e.*, d and π electrons. Thus, we carried out STM/STS simulations around the Fermi level [Fig. 4(b)]. The d$I$/d$V$ spectra display two prominent Hubbard peaks below and above the Fermi level with itinerant peaks right at the Fermi level. The STM topographies at the upper/lower Hubbard peak with a bias of 0.45/−1.55 eV exhibit clear kagome patterns, and a honeycomb feature is observed for the bias of 0 eV around the itinerant peaks [insets of Fig. 4(b)]. Moreover, using the spin-polarized STM/STS (SP-STM/STS),[49–51] phase evolution between different quantum states can potentially be directly measured (see the discussion in the ESI and Fig. S4†)

Because the feature of dichotomy has not been directly observable so far, the corresponding mechanisms proposed cannot be confirmed. For example, the GMR effect has been explained by the formation of "magnetic polarons",[52–54] while the magnetic polaron has not been observed. We propose that 2D MOFs provide an ideal platform to demonstrate a direct connection between the magnetic polaron and GMR effect with feasible SP-STM/STS measurements. The key ingredient for the formation of the magnetic polaron has been known, which is a much stronger FM Hund's coupling $J_H$ than exchange coupling $J_d$.[11,55–57] This is exactly the case for $Cu_3(HAB)_2$ [$J_H$ (100 meV) ≫ $J_d$ (7 meV)], similar to that in the doped EuTe[9,11,55] and colossal MR manganite systems.[58–60]

Under AFM background formed by Cu local spins, conjugated electrons polarize the surrounding Cu spins on the kagome lattice to form a magnetic polaron due to the strong Hund's coupling [Fig. 4(c)]. Since the conjugated electrons are also in a frustrated state, the magnetic polaron has a relatively smaller size. Consequently, the local spin misalignment strongly impedes electron movements, yielding an extremely high resistance. Applying a magnetic field, all the local spins are aligned parallel and the magnetic polaron disappears [Fig. 4(d)]. The system becomes an FM metallic state with very low resistance, giving rise to the GMR effect. These two different spin configurations with and without magnetic field

can be directly identified using SP-STM/STS (see the discussion in the ESI and Fig. S4†) and the GMR effect can also be experimentally observed with MR measurements.

## Conclusion and perspective

In summary, we have theoretically demonstrated a dichotomy between local spins and itinerant electrons in a 2D MOF for the first time. Most importantly, we propose that the dichotomy feature as well as the phase evolution of this intriguing system can be directly monitored through STM/STS and SP-STM/STS. Consequently, the underlying mechanisms of some intriguing physical manifestations can be better understood, such as the GMR effect due to the formation of magnetic polarons. We envision that strong correlated physics can be further explored through interdisciplinary efforts in MOFs, such as those resulting from frustration of both local and itinerant degrees of freedom. Our work suggests a new organic material platform for discovering new quantum physics as well as novel applications.

## Conflicts of interest

There are no conflicts of interest to declare.

## Acknowledgements

This project was supported by U.S. DOE-BES (Grant No. DE-FG02-04ER46148). W. J. was additionally supported by the NSF-Material Research Science & Engineering Center (Grand No. DMR-1121252). Z. L. was supported by the NSFC under Grant No. 11774196. We thank the CHPC at the University of Utah and DOE-NERSC for providing the computing resources.

## References

1 J. Kondo, *Prog. Theor. Phys.*, 1964, **32**, 37–49.
2 P. W. Anderson, *Phys. Rev.*, 1961, **124**, 41–53.
3 K. Andres, J. E. Graebner and H. R. Ott, *Phys. Rev. Lett.*, 1975, **35**, 1779–1782.
4 T. Senthil, M. Vojta and S. Sachdev, *Phys. Rev. B: Condens. Matter Mater. Phys.*, 2004, **69**, 035111.
5 J. G. Bednorz and K. A. Müller, *Z. Phys. B: Condens. Matter*, 1986, **64**, 189–193.
6 P. A. Lee, N. Nagaosa and X.-G. Wen, *Rev. Mod. Phys.*, 2006, **78**, 17–85.
7 J. Dai, Q. Si, J.-X. Zhu and E. Abrahams, *Proc. Natl. Acad. Sci. U. S. A.*, 2009, **106**, 4118–4121.
8 J.-W. Mei, S. Kawasaki, G.-Q. Zheng, Z.-Y. Weng and X.-G. Wen, *Phys. Rev. B: Condens. Matter Mater. Phys.*, 2012, **85**, 134519.
9 N. F. Oliveira, S. Foner, Y. Shapira and T. B. Reed, *Phys. Rev. B: Solid State*, 1972, **5**, 2634–2646.
10 A. P. Ramirez, *J. Phys.: Condens. Matter*, 1997, **9**, 8171.
11 D. Emin, *Polarons*, Cambridge University Press, 2013.
12 H.-C. Zhou, J. R. Long and O. M. Yaghi, *Chem. Rev.*, 2012, **112**, 673–674.
13 N. Stock and S. Biswas, *Chem. Rev.*, 2012, **112**, 933–969.
14 M. OKeeffe and O. M. Yaghi, *Chem. Rev.*, 2012, **112**, 675–702.
15 L. J. Murray, M. Dinca and J. R. Long, *Chem. Soc. Rev.*, 2009, **38**, 1294–1314.
16 J. Lee, O. K. Farha, J. Roberts, K. A. Scheidt, S. T. Nguyen and J. T. Hupp, *Chem. Soc. Rev.*, 2009, **38**, 1450–1459.
17 J.-R. Li, R. J. Kuppler and H.-C. Zhou, *Chem. Soc. Rev.*, 2009, **38**, 1477–1504.
18 P. Deria, J. E. Mondloch, O. Karagiaridi, W. Bury, J. T. Hupp and O. K. Farha, *Chem. Soc. Rev.*, 2014, **43**, 5896–5912.
19 C. K. Brozek and M. Dinca, *Chem. Soc. Rev.*, 2014, **43**, 5456–5467.
20 Y. J. Colon and R. Q. Snurr, *Chem. Soc. Rev.*, 2014, **43**, 5735–5749.
21 T. Kambe, R. Sakamoto, K. Hoshiko, K. Takada, M. Miyachi, J.-H. Ryu, S. Sasaki, J. Kim, K. Nakazato, M. Takata and H. Nishihara, *J. Am. Chem. Soc.*, 2013, **135**, 2462–2465.
22 D. Sheberla, L. Sun, M. A. Blood-Forsythe, S. Er, C. R. Wade, C. K. Brozek, A. Aspuru-Guzik and M. Dincă, *J. Am. Chem. Soc.*, 2014, **136**, 8859–8862.
23 M. G. Campbell, D. Sheberla, S. F. Liu, T. M. Swager and M. Dincă, *Angew. Chem., Int. Ed.*, 2015, **54**, 4349–4352.
24 Z. F. Wang, N. Su and F. Liu, *Nano Lett.*, 2013, **13**, 2842–2845.
25 Z. Liu, Z.-F. Wang, J.-W. Mei, Y.-S. Wu and F. Liu, *Phys. Rev. Lett.*, 2013, **110**, 106804.
26 M. G. Yamada, T. Soejima, N. Tsuji, D. Hirai, M. Dincă and H. Aoki, *Phys. Rev. B: Condens. Matter Mater. Phys.*, 2016, **94**, 081102.
27 H. Chen, S. Zhang, W. Jiang, C. Zhang, H. Guo, Z. Liu, Z. Wang, F. Liu and X. Niu, *J. Mater. Chem. A*, 2018, **6**, 11252–11259.
28 X. Ni, W. Jiang, H. Huang, K.-H. Jin and F. Liu, *Nanoscale*, 2018, **10**, 11901–11906.
29 N. Lahiri, N. Lotfizadeh, R. Tsuchikawa, V. V. Deshpande and J. Louie, *J. Am. Chem. Soc.*, 2017, **139**, 19–22.
30 J.-H. Dou, L. Sun, Y. Ge, W. Li, C. H. Hendon, J. Li, S. Gul, J. Yano, E. A. Stach and M. Dincă, *J. Am. Chem. Soc.*, 2017, **139**, 13608–13611.
31 D. T. Sawyer, G. S. Srivatsa, M. E. Bodini, W. P. Schaefer and R. M. Wing, *J. Am. Chem. Soc.*, 1986, **108**, 936–942.
32 P. Chaudhuri, C. N. Verani, E. Bill, E. Bothe, T. Weyhermüller and K. Wieghardt, *J. Am. Chem. Soc.*, 2001, **123**, 2213–2223.
33 V. Bachler, G. Olbrich, F. Neese and K. Wieghardt, *Inorg. Chem.*, 2002, **41**, 4179–4193.
34 K. Ray, T. Weyhermüller, F. Neese and K. Wieghardt, *Inorg. Chem.*, 2005, **44**, 5345–5360.

 

35 N. Su, W. Jiang, Z. Wang and F. Liu, *Appl. Phys. Lett.*, 2018, **112**, 033301.
36 C. Wu, D. Bergman, L. Balents and S. Das Sarma, *Phys. Rev. Lett.*, 2007, **99**, 070401.
37 W. Jiang, H. Huang, J.-W. Mei and F. Liu, *Phys. Chem. Chem. Phys.*, 2018, **20**, 21693–21698.
38 W. Jiang, M. Zhou, Z. Liu, D. Sun, Z. V. Vardeny and F. Liu, *J. Phys.: Condens. Matter*, 2016, **28**, 176004.
39 T. Kambe, R. Sakamoto, T. Kusamoto, T. Pal, N. Fukui, K. Hoshiko, T. Shimojima, Z. Wang, T. Hirahara, K. Ishizaka, S. Hasegawa, F. Liu and H. Nishihara, *J. Am. Chem. Soc.*, 2014, **136**, 14357–14360.
40 X. Sun, K.-H. Wu, R. Sakamoto, T. Kusamoto, H. Maeda, X. Ni, W. Jiang, F. Liu, S. Sasaki, H. Masunaga and H. Nishihara, *Chem. Sci.*, 2017, **8**, 8078–8085.
41 E. J. H. Phua, K.-H. Wu, K. Wada, T. Kusamoto, H. Maeda, J. Cao, R. Sakamoto, H. Masunaga, S. Sasaki, J.-W. Mei, W. Jiang, F. Liu and H. Nishihara, *Chem. Lett.*, 2018, **47**, 126–129.
42 Y. Kato, I. Martin and C. D. Batista, *Phys. Rev. Lett.*, 2010, **105**, 266405.
43 Y. Akagi, M. Udagawa and Y. Motome, *Phys. Rev. Lett.*, 2012, **108**, 096401.
44 S. Ghosh, P. O'Brien, C. L. Henley and M. J. Lawler, *Phys. Rev. B: Condens. Matter Mater. Phys.*, 2016, **93**, 024401.
45 N. Lin, A. Langner, S. L. Tait, C. Rajadurai, M. Ruben and K. Kern, *Chem. Commun.*, 2007, 4860–4862.
46 S. L. Tait, A. Langner, N. Lin, R. Chandrasekar, O. Fuhr, M. Ruben and K. Kern, *ChemPhysChem*, 2008, **9**, 2495–2499.
47 L. Bartels, *Nat. Chem.*, 2010, **2**, 87–95.
48 A. Kumar, K. Banerjee, A. S. Foster and P. Liljeroth, *Nano Lett.*, 2018, **18**, 5596–5602.
49 M. Bode, *Rep. Prog. Phys.*, 2003, **66**, 523.
50 S. Krause, L. Berbil-Bautista, G. Herzog, M. Bode and R. Wiesendanger, *Science*, 2007, **317**, 1537.
51 J. Wang, A. Deloach, W. Jiang, C. M. Papa, M. Myahkostupov, F. N. Castellano, F. Liu and D. B. Dougherty, *Phys. Rev. B: Condens. Matter Mater. Phys.*, 2017, **95**, 241410.
52 E. Nagaev, *ZhETF Pisma Redaktsiiu*, 1967, **6**, 484.
53 T. Kasuya, A. Yanase and T. Takeda, *Solid State Commun.*, 1970, **8**, 1543–1546.
54 M. Umehara and T. Kasuya, *J. Phys. Soc. Jpn.*, 1972, **33**, 602–615.
55 A. Mauger and D. L. Mills, *Phys. Rev. B: Condens. Matter Mater. Phys.*, 1985, **31**, 8024–8033.
56 A.-M. Haghiri-Gosnet and J.-P. Renard, *J. Phys. D: Appl. Phys.*, 2003, **36**, R127.
57 N. Mannella, W. L. Yang, K. Tanaka, X. J. Zhou, H. Zheng, J. F. Mitchell, J. Zaanen, T. P. Devereaux, N. Nagaosa, Z. Hussain and Z.-X. Shen, *Phys. Rev. B: Condens. Matter Mater. Phys.*, 2007, **76**, 233102.
58 A. Urushibara, Y. Moritomo, T. Arima, A. Asamitsu, G. Kido and Y. Tokura, *Phys. Rev. B: Condens. Matter Mater. Phys.*, 1995, **51**, 14103–14109.
59 C. N. R. Rao, A. K. Cheetham and R. Mahesh, *Chem. Mater.*, 1996, **8**, 2421–2432.
60 Y. Moritomo, A. Asamitsu, H. Kuwahara and Y. Tokura, *Nature*, 1996, **380**, 141–144.